PCP
PLANT & CELL PHYSIOLOGY

Special Focus Issue – Regular Paper

Visualization of Uptake of Mineral Elements and the Dynamics of Photosynthates in Arabidopsis by a Newly Developed Real-Time Radioisotope Imaging System (RRIS)

Ryohei Sugita[1], Natsuko I. Kobayashi[1], Atsushi Hirose[1], Takayuki Saito[2], Ren Iwata[3], Keitaro Tanoi[1,4] and Tomoko M. Nakanishi[1,*]

[1]Graduate School of Agricultural and Life Sciences, The University of Tokyo, 1-1-1, Yayoi, Bunkyo-ku, Tokyo, 113-8657 Japan
[2]AgroSolutions Division-Japan, Sumitomo Chemical Co., Ltd., 4-6-1, Ichibancho, Aoba-ku Sendai, Miyagi, 980-0811 Japan
[3]Cyclotron and Radioisotope Center (CYRIC), Tohoku University, 6-3, Aoba, Aramaki, Aoba-ku, Sendai, Miyagi, 980-8578 Japan
[4]PRESTO, Japan Science and Technology Agency (JST), 4-1-8 Honcho, Kawaguchi, Saitama, 332-0012 Japan
*Corresponding author: E-mail, atomoko@mail.ecc.u-tokyo.ac.jp, Fax, +81-3-5841-8193.
(Received August 30, 2015; Accepted March 14, 2016)

Minerals and photosynthates are essential for many plant processes, but their imaging in live plants is difficult. We have developed a method for their live imaging in Arabidopsis using a real-time radioisotope imaging system. When each radioisotope, ^{22}Na, ^{28}Mg, ^{32}P-phosphate, ^{35}S-sulfate, ^{42}K, ^{45}Ca, ^{54}Mn and ^{137}Cs, was employed as an ion tracer, ion movement from root to shoot over 24 h was clearly observed. The movements of ^{22}Na, ^{42}K, ^{32}P, ^{35}S and ^{137}Cs were fast so that they spread to the tip of stems. In contrast, high accumulation of ^{28}Mg, ^{45}Ca and ^{54}Mn was found in the basal part of the main stem. Based on this time-course analysis, the velocity of ion movement in the main stem was calculated, and found to be fastest for S and K among the ions we tested in this study. Furthermore, application of a heat-girdling treatment allowed determination of individual ion movement via xylem flow alone, excluding phloem flow, within the main stem of 43-day-old Arabidopsis inflorescences. We also successfully developed a new system for visualizing photosynthates using labeled carbon dioxide, $^{14}CO_2$. Using this system, the switching of source/sink organs and phloem flow direction could be monitored in parts of whole shoots and over time. In roots, ^{14}C photosynthates accumulated intensively in the growing root tip area, 200–800 μm behind the meristem. These results show that this real-time radioisotope imaging system allows visualization of many nuclides over a long time-course and thus constitutes a powerful tool for the analysis of various physiological phenomena.

Keywords: Arabidopsis • Live imaging • Mineral elements • Photosynthates • Real-time radioisotope imaging system • Sink–source switching.

Abbreviations: CCD, charge-coupled device; FOS, fiber optic plate with scintillator; IP, imaging plate; LOQ, limit of quantitation; MGRL, Molecular Genetics Research Laboratory; MRI, magnetic resonance imaging; PET, positron emission tomography; PETIS, positron-emitting tracer imaging system; PlanTIS, plant tomographic imaging system; ROI, region of interest; RRIS, real-time radioisotope imaging system.

Introduction

To elucidate the mechanisms of growth, metabolism and response to stresses in living organisms, it is important also to study the dynamics of substances expected to be involved in these processes. To analyze the movement of substances in live plants, it is best to employ non-destructive methods such as fluorescence, chemiluminescence, infrared light and radiation measurements. However, techniques employing fluorescence and chemiluminescence present difficulties in observing substance movement in a whole plant body. In addition, fluorescence imaging of living plants is further confounded by the fact that light is essential for plant growth, and as such it is difficult to observe substances non-destructively via these methods. Therefore, radioisotope imaging is an ideal method to visualize substance dynamics in living plants as well as in other organisms.

In medical diagnostics, a special kind of radioisotope, the positron emitter, is widely used as an imaging method known as positron emission tomography (PET) (Phelps et al. 2000, Antoch et al. 2003, Schaller 2004). There have been several reports of the application of positron-emitting nuclides for imaging the dynamics of substances in a living plant, and some attempts have combined them with other imaging methods. For instance, the plant tomographic imaging system (PlanTIS) in which a three-dimensional magnetic resonance imaging (MRI) image is superimposed on a PET image to obtain higher resolution has been proposed (Jahnke et al. 2009, De Schepper et al. 2013). Several imaging systems based on positron imaging have been applied to mobile apparatus equipped with small detectors: the PhytoBeta imager (Weisenberger et al. 2012), a wide area (20×30 cm) imaging system called Duke VIPER (versatile imager for positron emitting radiotracers) (Kiser et al. 2008) and a positron emitting tracer imaging system (PETIS) (Fujimaki et al. 2010).

Plant Cell Physiol. 57(4): 743–753 (2016) doi:10.1093/pcp/pcw056, Advance Access publication on 24 March 2016, available online at www.pcp.oxfordjournals.org

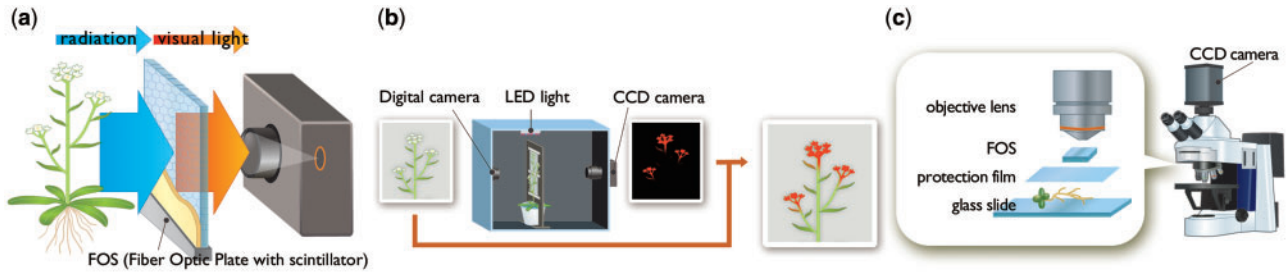

Fig. 1 Outline of the real-time radioisotope imaging system (RRIS). (a) The radiation was converted to visual light by a CsI (Tl) scintillator deposited on a FOS. The light was introduced to a high-sensitivity CCD camera to produce the radiation profile image. (b) The camera was equipped with a dark box (60×40×40 cm) in which plants were grown. To superimpose a true image on the RRIS image, the digital camera was installed on the other side of the CCD camera. (c) Schematic of the micro-RRIS. To obtain a higher resolution image, RRIS was combined with a microscope.

The phoswich imaging detector (Wu and Tai 2011) was developed to allow both positron- and γ-ray-emitting nuclide imaging. Studies using live imaging systems, including PlanTIS and PETIS, have investigated the movement of radionuclides in tomato (Suwa et al. 2008), broadbean (Matsuhashi et al. 2005), beet and bulbs (Jahnke et al. 2009), soybean (Kawachi et al. 2011), barley (Tsukamoto et al. 2006), wheat (Matsuhashi et al. 2006) and rice (Ishikawa et al. 2011). The positron emitters used for these imaging systems were ^{11}C (Minchin and Thorpe 2003), ^{13}N (Ohtake et al. 2001), ^{15}O (Kiyomiya et al. 2001), ^{18}F (Nakanishi et al. 2001), ^{52}Fe (Tsukamoto et al. 2009), ^{52}Mn (Tsukamoto et al. 2006) and ^{107}Cd (Fujimaki et al. 2010).

We previously developed a real-time radioisotope imaging system (RRIS) to visualize ion movement in plants (Nakanishi et al. 2009). A schematic illustration of the imaging system is shown in **Fig. 1**. When a radioisotope is supplied to the plant, it emits radiation. The radiation is converted to visual light by a CsI (Tl) scintillator deposited on a fiber optic plate (FOS) (Hamamatsu Photonics Co.). The light is led to a highly sensitive charge-coupled device (CCD) camera to produce a radiation profile image. To date, two imaging systems, macro-RRIS and micro-RRIS, have been developed. The former can image an area of 20×10 cm, and the latter can visualize radioisotope (^{109}Cd) movement under a microscope at a resolution of at most 500 μm (Kanno et al. 2012). RRIS enables the imaging of various types of radiation including β, γ and X-rays (Sugita et al. 2014). Consequently, live imaging of several essential elements such as phosphorus (^{32}P, ^{33}P) and sulfur (^{35}S) is possible (Nakanishi et al. 2011, Kanno et al. 2012).

In the present study, we applied RRIS to the study of long-distance ion transport in plants. After ion absorption by roots, transpiration flow and root pressure provide the driving force for root-to-shoot transport via the xylem (Marschner 1995). Various ion channels with unique characteristics are thought to underlie ion-specific transport systems (Véry and Sentenac 2003, Yamaji and Ma 2009); however, in vivo ion-specific long-distance transport mechanisms have not been identified. For this purpose, RRIS can be an effective tool, given its ability to detect a rich variety of radioisotopes. We therefore visualized the comparative transport kinetics of the main macronutirents: ^{22}Na, ^{28}Mg, ^{32}P, ^{35}S, ^{42}K, ^{45}Ca, ^{54}Mn and ^{137}Cs, in the model plant *Arabidopsis thaliana*. In addition, imaging experiments using radiolabeled $^{14}CO_2$ as a gas were performed to visualize the dynamics of photosynthates and thus characterize phloem flow in Arabidopsis.

Results

Visualization of eight elements from roots to above-ground parts in 43-day-old Arabidopsis plants

Eight ions, $^{22}Na^+$, $^{28}Mg^{2+}$, ^{32}P-phosphate, ^{35}S-sulfate, $^{42}K^+$, $^{45}Ca^{2+}$, $^{54}Mn^{2+}$ and $^{137}Cs^+$, were supplied to roots and within 24 h the accumulation pattern and uptake speed of each element exhibited specific features (**Fig. 2a, b**). Successive figures were connected to show the movement pattern of each element (see **Supplementary videos** 22Na.avi, 28Mg.avi, 32P.avi, etc.). Sequential analysis showed two distribution patterns in the above-ground parts. The first was a widespread distribution over time, as exhibited by ^{22}Na, ^{32}P, ^{35}S, ^{42}K and ^{137}Cs. The second pattern shown by elements ^{28}Mg, ^{45}Ca and ^{54}Mn, was a higher accumulation in the basal part of the main stem (**Fig. 2b**), indicating a curved distribution pattern of tracers (**Fig. 2c**). Surprisingly, no ^{45}Ca or ^{54}Mn, and little ^{28}Mg reached the tip of the stem, even after 24 h. The transport kinetics of ^{28}Mg, ^{32}P, ^{35}S and ^{42}K within the main stem of the inflorescence were further characterized by analyzing the temporally increasing radioactivity in the two regions of interest (ROIs) separated by a distance of 30 mm (**Fig. 2d**). The signal intensity of ^{28}Mg in the ROI:A, which was set at the lower position, exceeded the limit of quantitation (LOQ) soon after sequential imaging was started and continued to increase linearly (**Fig. 2d**: 1, 2, 3, 4). The LOQ corresponds to the earliest time that each radioisotope can first be detected. Subsequently, after approximately 6 h, the ^{28}Mg content in the ROI:B, which was set at the higher position, began to increase linearly (**Fig. 2d**: 1, 2). According to the time gap between ROI:A and ROI:B to reach the LOQ of ^{28}Mg, the time required for ^{28}Mg to travel 30 mm was 5.5 h (experiment 1: **Fig. 2d**: 3) and 3.0 h (experiment 2: **Fig. 2d**: 4). Accordingly, the velocities of Mg^{2+} toward the top of the main stem were estimated to be 5.5 mm h^{-1} (experiment 1: **Fig. 2d**: 3)

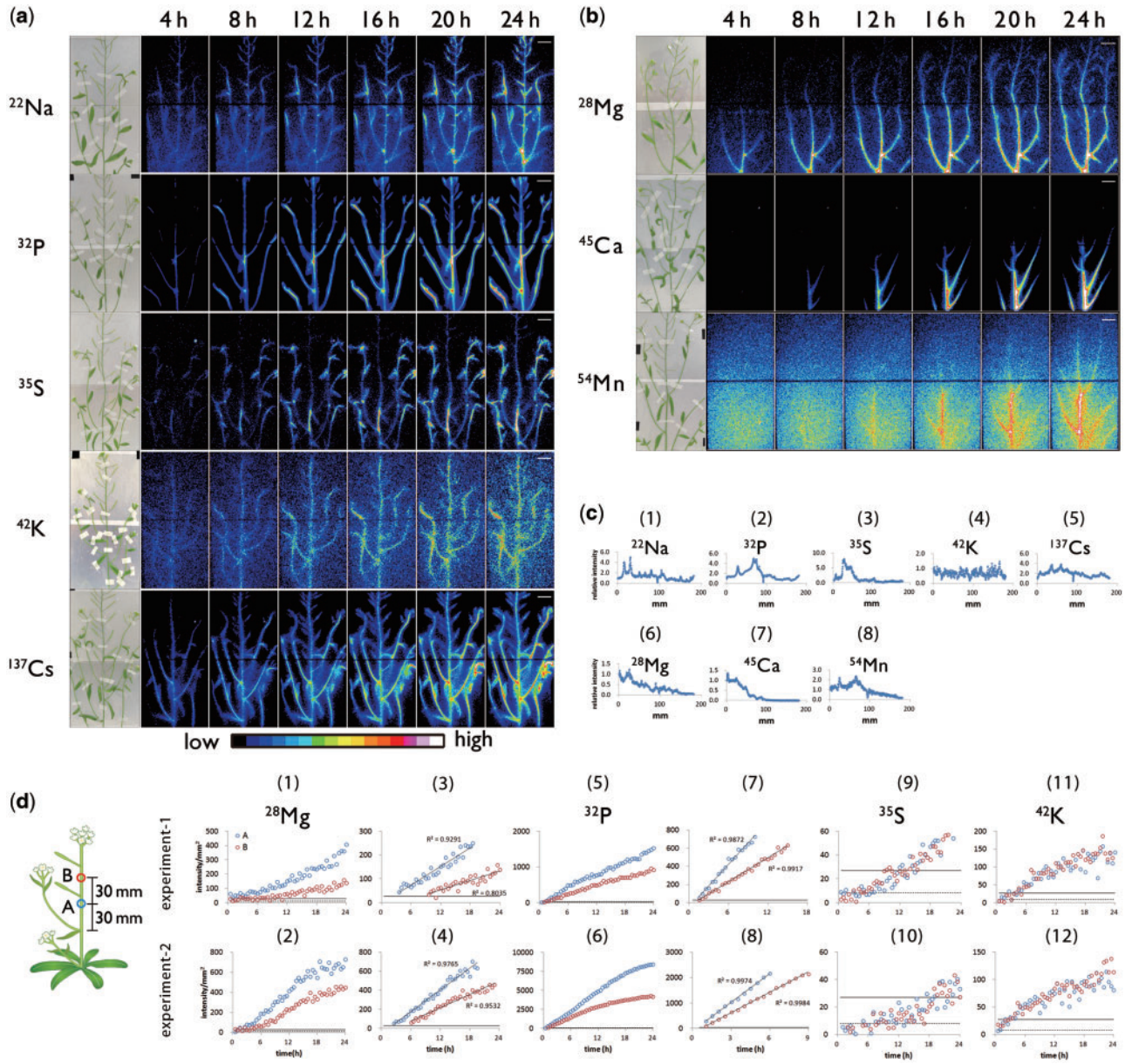

Fig. 2 Photograph of test plants and serial images of ion movement taken by macro-RRIS. Macro-RRIS images of (a) ^{22}Na, ^{32}P-phosphate, ^{35}S-sulfate, ^{42}K and ^{137}Cs, (b) ^{28}Mg, ^{45}Ca and ^{54}Mn supplied to roots. The detection time for each image was set to 15 min. Scale bar = 2 cm. (c) The distribution profile after 24 h absorption of radiotracers in the shoot acquired by the macro-RRIS experiments. (d) Time-course analysis of the radioactivity of ^{28}Mg (1–4), ^{32}P (5–8), ^{35}S (9, 10) and ^{42}K (11, 12) detected in two ROIs. ROI:A, surrounded by a blue circle, was set on the main stem of the 30 mm upper part from the top node. ROI:B, surrounded by a red circle, was placed apart by 30 mm from the ROI:A. For each individual radiotracer study, two experiments were performed, and the results were vertically arranged. The solid line shows the limit of quantitation (LOQ). The broken line shows the limit of detection. The linear components in (1), (2), (5) and (6) were extracted in (3), (4), (7) and (8), respectively.

and 10.0 mm h^{-1} (experiment 2: **Fig. 2d**: 4). In contrast, the difference between the times when the ^{32}P signal was first detected in ROI:A and ROI:B was <30 min (**Fig. 2d**: 7, 8); thus, the velocity of P was calculated to be >60 mm h^{-1}. For ^{35}S and ^{42}K, after the signal intensities in the two ROIs exceeded the LOQ, they increased similarly, indicating that the velocities of these ions were too great to be estimated under the current experimental conditions.

Discrimination between xylem and phloem flow using girdling

In the inflorescence, both xylem and phloem flow can affect ion transport. To determine ion movement via the xylem, we assessed the transport and distribution of ^{28}Mg and ^{32}P in which phloem flow in the main stem was inhibited by heat-girdling (**Fig. 3**). The inhibitory effect of heat-girdling on phloem flow in the main stem was assessed by the distribution of ^{14}C-labeled

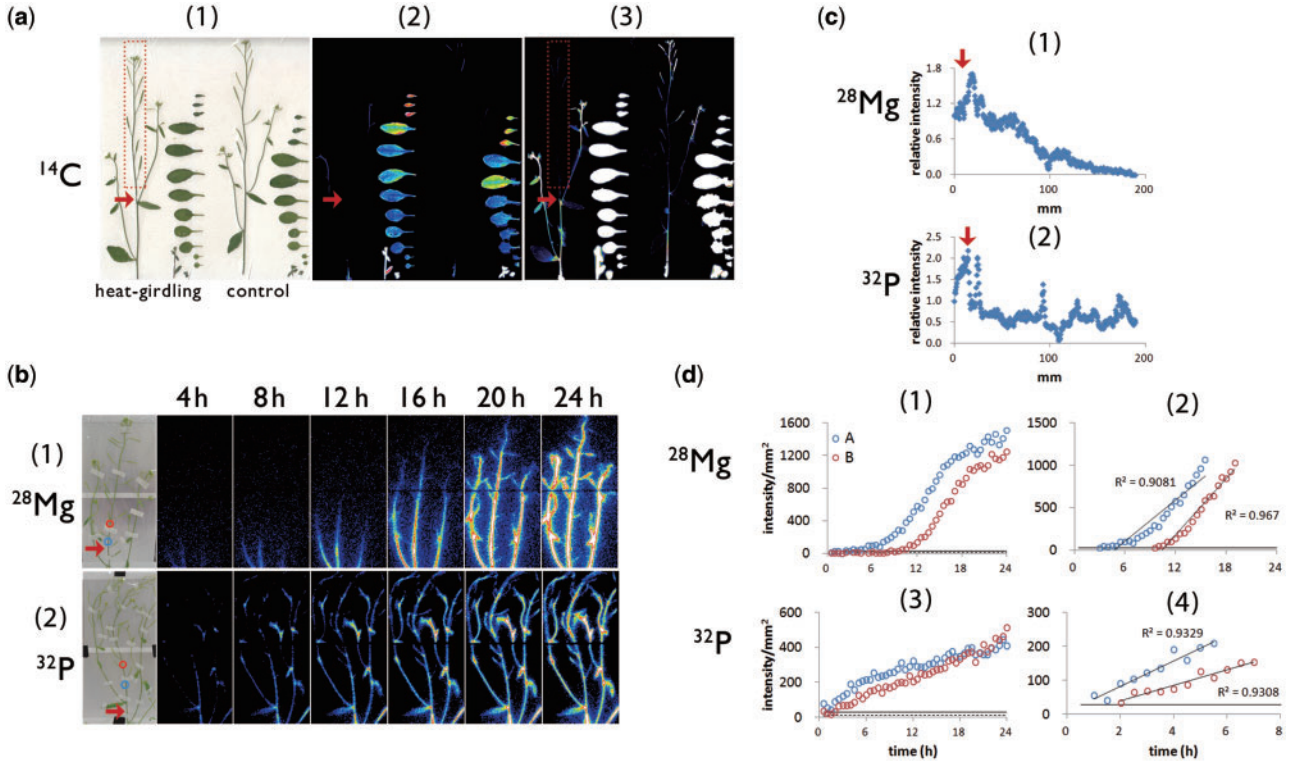

Fig. 3 Heat-girdling treatment to discriminate the xylem flow from the phloem flow. (a) ^{14}C distribution images acquired by the imaging plate after heat-girdling treatment applied to the Arabidopsis main stem (red arrows) confirmed that the heat-girdling treatment successfully inhibited the phloem flow directed to the apical part of the main stem. $^{14}CO_2$ was supplied to rosette leaves. (1) Sample picture, (2) ^{14}C distribution images acquired by an imaging plate, (3) brightness of the center images was enhanced so that the ^{14}C signal in the inflorescence was visible. (b) Macro-RRIS images of ^{28}Mg and ^{32}P in Arabidopsis with the heat-girdling treatment at the position marked with the red arrows. The exposure time of the camera was set to 15 min. ROIs were indicated with the blue circle (ROI: A) and red circle (ROI:B) in the image. (c) The distribution profile of ^{28}Mg (1) and ^{32}P (2) along the main stem after 16 h absorption of radiotracers acquired by the macro-RRIS experiments shown in (b). The position of the heat-girdling treatment was marked with the red arrow. *x*-axis, the distance (mm) from the bottom part of the inflorescence. (d) Time course of ^{28}Mg (1, 2) and ^{32}P (3, 4) signal intensity in ROI:A (blue circle) and ROI:B (red circle) as illustrated in **Fig. 2d**. The linear components in (1) and (3) were extracted in (2) and (4), respectively.

photosynthates (**Fig. 3a**). After $^{14}CO_2$ was supplied to rosette leaves, the accumulation of ^{14}C signal in the apical stem was shown to be abolished by heat-girdling (**Fig. 3a**), thus indicating the reliability of our heat-girdling technique. Further, ^{28}Mg displayed a distribution pattern along the main stem that was similar to that of non-treated plants (**Figs. 2c**: 6, **3b**: 1, **3c**: 1). A kinetic analysis showed that the velocity of Mg^{2+} in the xylem flow was 5.5 mm h^{-1} (**Fig. 3d**: 2), a value in the range of that found in intact Arabidopsis (**Fig. 2d**: 3, 4). Thus, the upward Mg^{2+} movement within the third internode of the main stem is likely to be mediated mainly by xylem flow, while the phloem contribution is scarce during the first 24 h of root absorption. In contrast, heat-girdling resulted in strong ^{32}P signal accumulation at the bottom of the main stem (**Fig. 3b**: 2, **3c**: 2), which was never observed in untreated Arabidopsis (**Fig. 2c**: 2). The difference in the time taken for the ^{32}P signal intensity per square millimeter to reach LOQ in ROI:A and in ROI:B was 1 h; thus, the velocity of P in the xylem stream was calculated to be 30 mm h^{-1}(**Fig. 3d**: 4), and thus slower than in intact plants (**Fig. 2d**: 7, 8). In addition, unlike in untreated Arabidopsis (**Fig. 2d**: 5, 6), the rate of increase of ^{32}P signal intensity in ROI:A as well as in ROI:B in plants with girdled inflorescences gradually decreased (**Fig. 3d**: 3). As a result, the ^{32}P radioactivity in ROI:A, which began to increase earlier than in ROI:B, reached the same level as for ROI:B after 18 h. These results suggest that the large signal increase in ROI:A observed after 5 h of imaging of intact plants (**Fig. 2d**: 5, 6) was due to phloem transport. In this context, the contribution of phloem flow to phosphate transport toward the shoot meristem could be significant even within 24 h of root absorption. Furthermore, based on our observation that the gap between ^{32}P radioactivity in ROI:A and that in ROI:B increased with time, phosphate transport via the phloem along the main stem was inferred to be slower than via the xylem.

The destination of phloem flow from rosette leaves

To investigate the sink–source relationship between rosette leaves and inflorescences, $^{14}CO_2$ was supplied to the rosette leaves of 43-day-old Arabidopsis plants, and the upward movement of ^{14}C-labeled photosynthates was visualized by RRIS (**Fig. 4a**). After live imaging for 24 h, samples were placed on

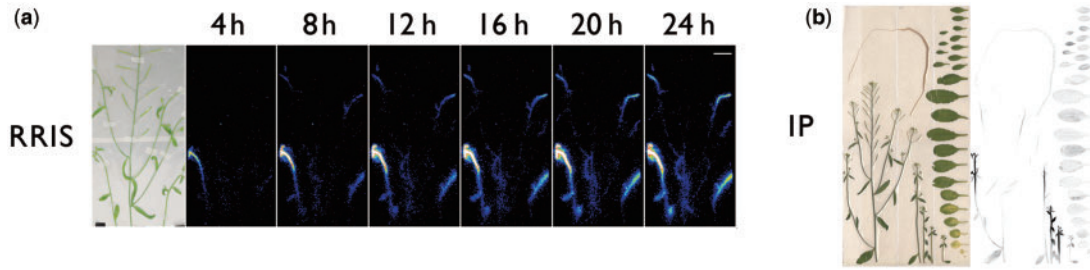

Fig. 4 Photograph of test plants and images of ^{14}C-labeled metabolite movement. (a) Macro-RRIS images of ^{14}C-labeled metabolite. $^{14}CO_2$ was supplied to rosette leaves. The detection was set at 15 min. Scale bar = 2 cm. (b) ^{14}C distribution images acquired by the imaging plate after the macro-RRIS experiment.

an imaging plate (IP), and a distribution image of ^{14}C throughout the plant was acquired (**Fig. 4b**). The amount of the ^{14}C-labeled metabolite at the main stem was very low, and hardly any signal appeared in the upper part of the main stem. From this, we inferred that rosette leaves were the source organs supplying photosynthates primarily to the lateral stems, while the phloem flow along the sieve tube connecting the basal shoot and the tip region of the main stem was minimal. This result was surprising given that sink parts such as developing flowers and siliques were present on the main stem. We therefore hypothesized that the rosette leaves are the source organs when the stem is young, but, after flowering, the necessary carbon source in the stem is supplied by photosynthates produced in siliques, stems and cauline leaves. To test this hypothesis, the same experiment was performed using a younger plant at 30 d after germination. Accordingly, the movement of the photosynthates was different from that in the 43-day-old plants (**Figs. 4a**, **5a**). The photosynthate produced in the rosette leaves was preferentially transferred to the main stem tip. The direction of phloem flow from rosette leaves towards each stem changed in the basal shoot region and was influenced by the age of the stems.

Phloem flow direction and the source–sink relationship between organs were further studied by analyzing the amounts of ^{14}C-labeled photosynthates accumulated in the tip areas of main and lateral stems (**Fig. 6**). When $^{14}CO_2$ was supplied under both pulsed and continuous conditions to the rosette leaves, the signal intensity at the main stem tip increased more than at the lateral stem tip (**Fig. 6**). In contrast, the amounts of ^{14}C detected at the tips of main and lateral stems did not differ when $^{14}CO_2$ was supplied to the whole shoots (**Fig. 6**). These observations suggested the existence of a source organ other than the rosette leaves supplying photosynthates to the lateral stems. To determine whether the potential source organ was the inflorescence, we supplied $^{14}CO_2$ in pulses to the inflorescence only, and found that the ^{14}C signal intensity in the lateral stems remained higher than that in the main stems, and the ^{14}C signal intensity in the lateral tips continued to increase for up to 20 h, but not in the main stem tip. One explanation for this is that ^{14}C-labeled photosynthates generated in the main stem are continuously transported towards lateral stems. In addition, the ^{14}C signal in cauline leaves of lateral stems decreased (**Fig. 6c**), although the total signal intensity of ^{14}C in cauline leaves and lateral stem tips was maintained (**Fig. 6d**). This observation might indicate that cauline leaves also act as a carbon source for lateral stem tips.

Autoradiographic data obtained by live imaging revealed a ^{14}C signal in roots when $^{14}CO_2$ was supplied to rosette leaves or whole shoots (**Fig. 7**). In contrast, no ^{14}C signal was observed in roots and rosette leaves when $^{14}CO_2$ was supplied to the inflorescences (**Fig. 7**). These results show that there is little phloem flow leaving the inflorescences and that the rosettes are the primary carbon source for roots. Thus the photosynthates fixed in the inflorescence seem to be transported, metabolized and accumulated only within the inflorescence itself.

Visualization of sink tissues within developing areas of the root

When gas was supplied to the rosette leaves, ^{14}C-labeled photosynthates were found to be transported to the root (**Fig. 7**). To determine the sink tissues within the roots, the downward movement of ^{14}C-labeled photosynthates was visualized after $^{14}CO_2$ was supplied only to above-ground parts of 2-week-old seedlings, which are juvenile plants before flowering (**Fig. 8a**). RRIS images of ^{14}C in roots show the arrival of ^{14}C-labeled photosynthates at the root tip areas involved in developing lateral roots as early as 3 h following $^{14}CO_2$ supply (**Fig. 8b**). Thereafter, the accumulation of ^{14}C-labeled photosynthates in lateral root tips increased for 12 h, and, after live imaging, the accumulation of ^{14}C-labeled photosynthates between 200 and 800 μm distal to the main root tip was also confirmed using micro-RRIS (**Fig. 8c**). The root elongation rate in 2-week-old Arabidopsis plants was 5.1 ± 0.4 (SD) mm during 12 h. Therefore, the root segments captured in **Fig. 8c** were inferred to be newly developed tissues constructed with the ^{14}C-labeled photosynthate.

Discussion

The distinct contributions of xylem and phloem flows to the transport of ions in the main inflorescence stem.

In this study, our imaging system was able to identify clearly ion-specific distribution patterns and transport velocities in the main stems of Arabidopsis plants within 24 h of root absorption

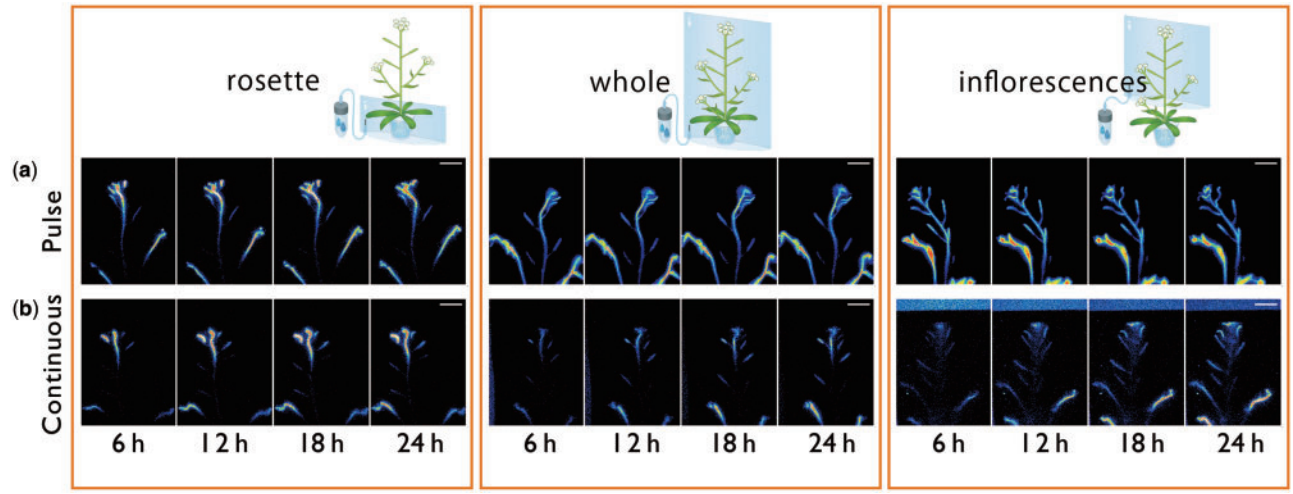

Fig. 5 Imaging of ^{14}C-labeled metabolite distribution after/while supplying the $^{14}CO_2$ either from rosette leaves, the whole part of the shoot or the inflorescence. Serial images of ^{14}C-labeled metabolite movement acquired by RRIS. Supply of $^{14}CO_2$ to the rosette, whole shoots and inflorescences was performed with (a) pulse–chase experiments and (b) continuous experiments. The imaging time for each frame was 15 min. Scale bar = 20 mm.

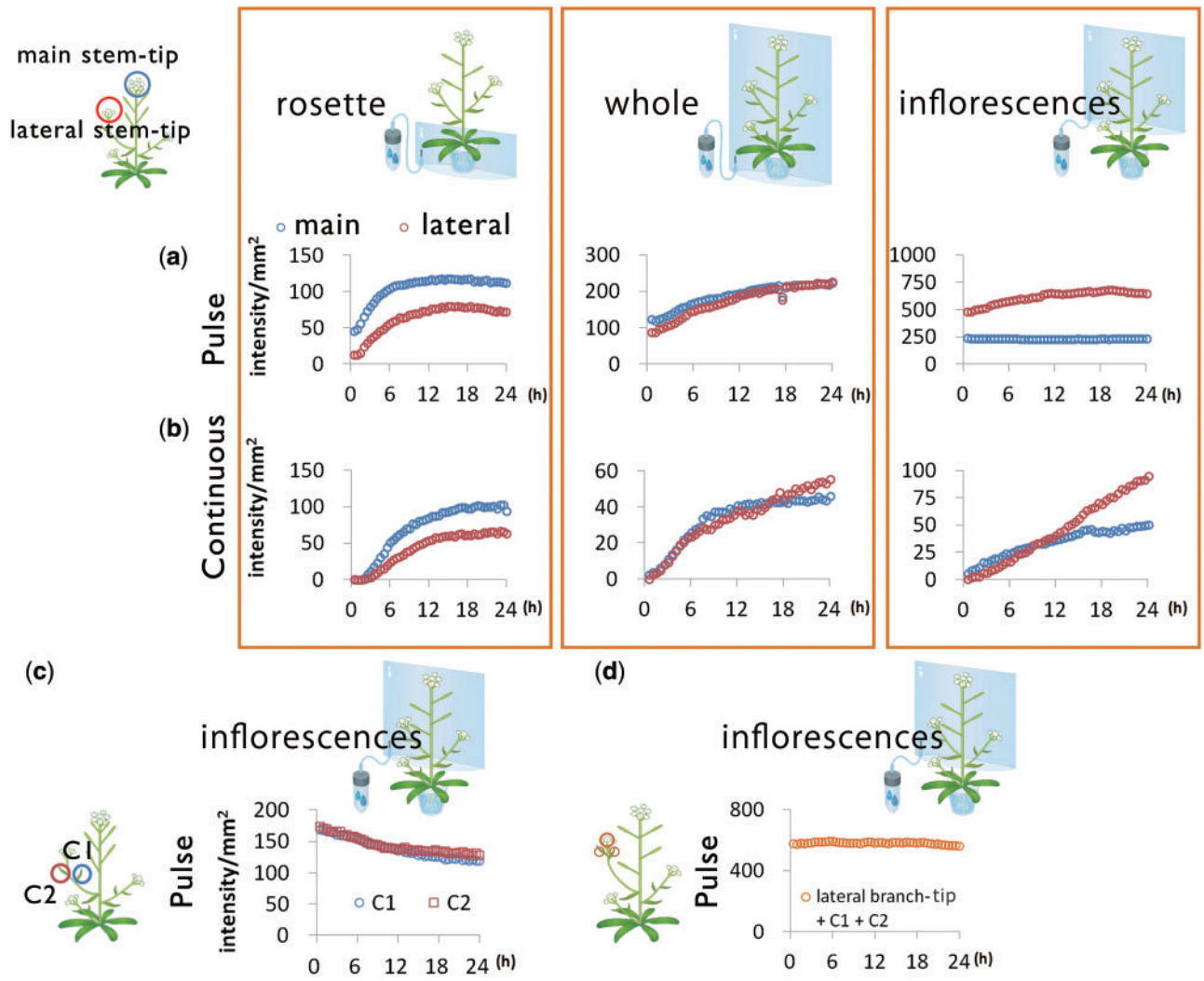

Fig. 6 Time-course analysis of ^{14}C-labeled metabolites. Time course of signal intensity of ^{14}C in ROI: main and lateral stem tip from rosette, whole shoots and inflorescences with (a) $^{14}CO_2$ pulse–chase experiments and (b) $^{14}CO_2$ continuous experiments. (c) Time course of signal intensity of ^{14}C in two ROIs set on the cauline leaves (C1 and C2) in the sequential images in (a). (d) Time course of total signal intensity of ^{14}C in three ROIs set on the cauline leaves and lateral stem tip in the sequential images in (a).

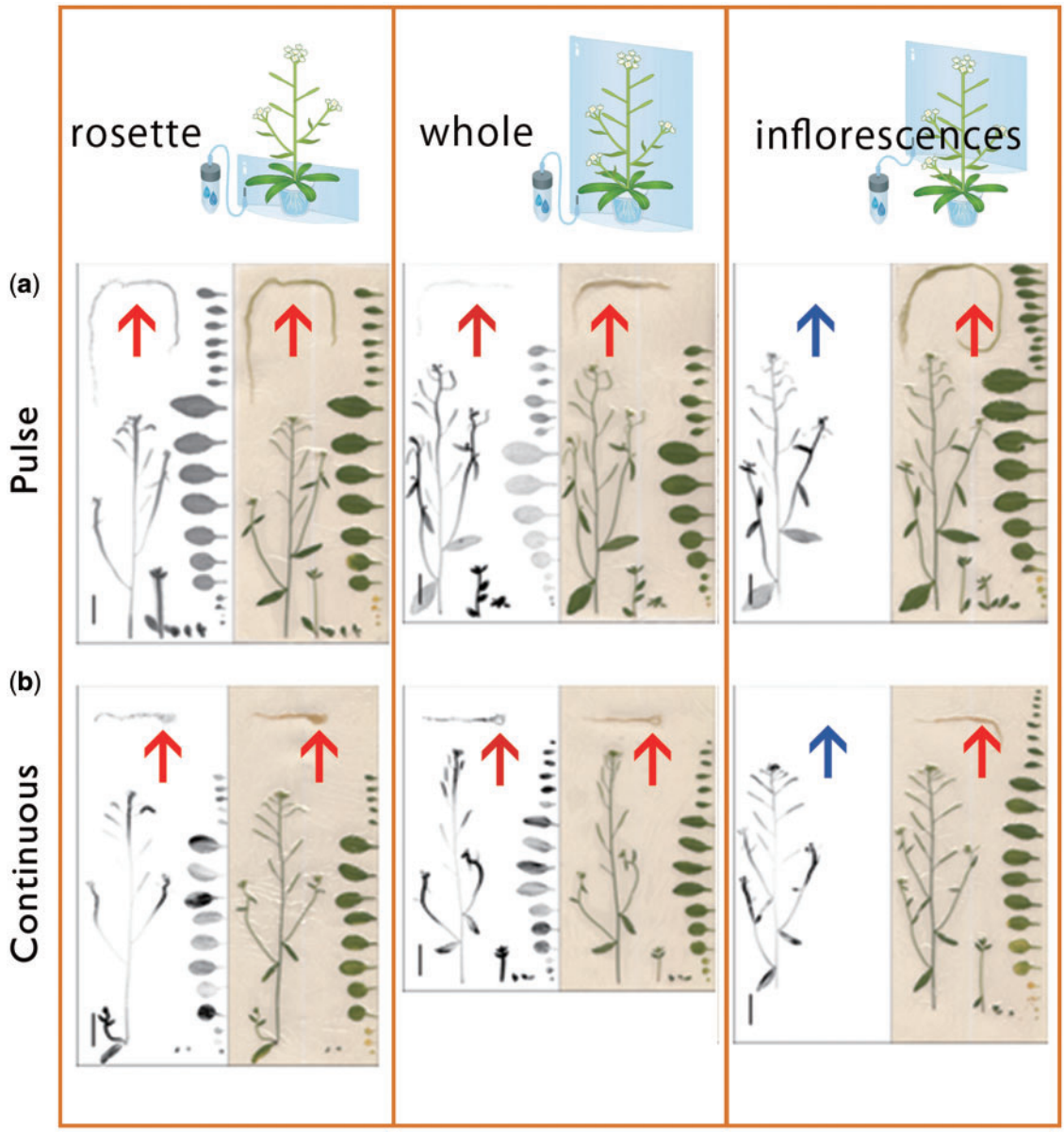

Fig. 7 Imaging of ^{14}C-labeled metabolite distribution pattern in Arabidopsis with three supply processings. The ^{14}C distribution images acquired with an imaging plate after RRIS and sample images are described. $^{14}CO_2$ supply to rosette, whole shoots and inflorescences was performed by (a) pulse–chase experiments and (b) continuous experiments. Scale bar = 20 mm. The arrow indicates a root.

(**Fig. 2**). The difference in distributions seemed to be derived, at least in part, from the chemical forms of the elements; one group comprised monovalent cations or anions (i.e ^{22}Na, ^{42}K, ^{32}P, ^{35}S and ^{137}Cs), whereas the other group are multivalent cations (i.e. ^{28}Mg, ^{45}Ca and ^{54}Mn). Given the widespread distribution profile along the main stem from the lower to the upper parts, monovalent cations and anions appeared to move through the vascular tissue smoothly and quickly (**Fig. 2c**), whereas multivalent cations moved slowly. After the ions reach the bottom part of the shoot, the part played by the phloem in promoting ion transport should be considered in addition to xylem flow. To evaluate phloem contribution to ion transport, heat-girdling was performed before image analysis of ^{28}Mg and ^{32}P. This revealed a slow upward transport of Mg^{2+} through the xylem, while we did not detect any Mg^{2+} transport via the phloem within 24 h of root absorption. The low velocity of multivalent cation transport (**Fig. 2b**) is possibly derived from the interaction between the ions and the negatively charged cell wall of xylem vessels, as was found in Cd transport in rice (Fujimaki et al. 2010). In addition, the ion-specific transport system around the xylem may lead to different mobilities of ions along the vascular tissue. Further, the amount of Mg and Ca pooled within xylem parenchyma cells during xylem transport was larger than that of K in climbing bean (Metzner et al. 2010). In contrast to Mg, P transport toward the tip of the main stem appeared to involve fast xylem transport and later phloem transport (**Figs. 2d**: 5, 6, **3d**: 3). Poor phloem flow from the basal shoot region towards the main stem in 43-day-old Arabidopsis

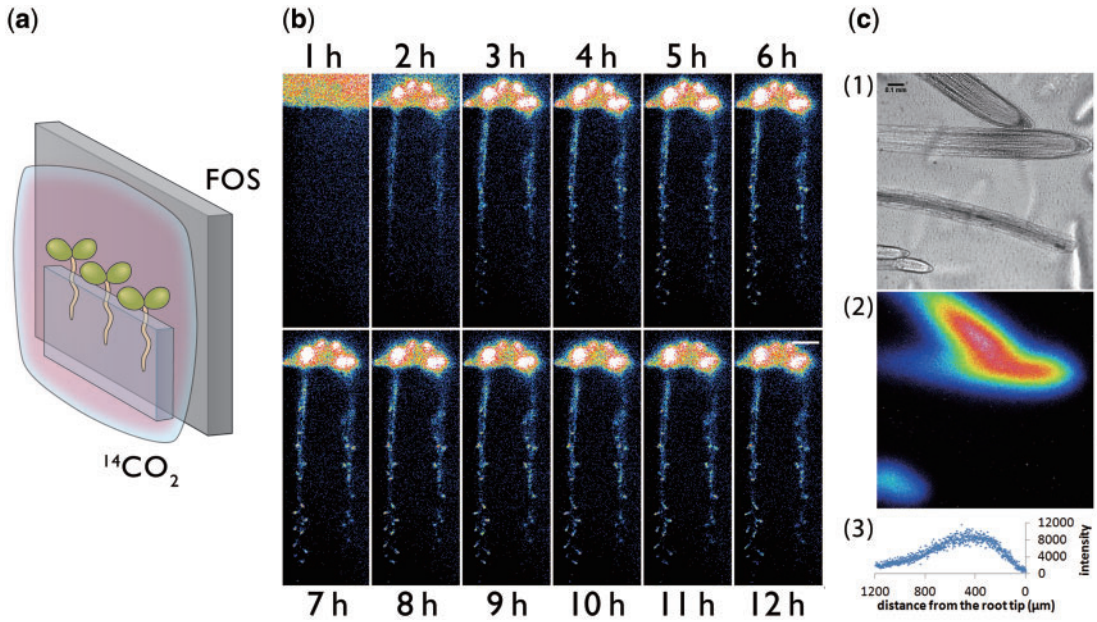

Fig. 8 Visualization of the downward movement of ^{14}C-labeled metabolites from leaves to roots. (a) Schematic of the photography method. Test plants were covered with a polyethylene bag for supply of $^{14}CO_2$. (b) Serial images of ^{14}C-labeled metabolite movement taken by macro-RRIS. Scale bar = 10 mm. (c) Micro-RRIS image of ^{14}C-labeled metabolites in the root (root tip, maturation area and lateral root), ^{14}C-labeled metabolite image and distribution profile of ^{14}C-labeled metabolites. Scale bar = 100 μm.

plants was also indicated by the photosynthate distribution analysis after the application of $^{14}CO_2$ to rosette leaves (**Fig. 4a, b**).

In the case of ^{35}S, higher amounts were found in the lateral stems compared with the main stem, a distribution pattern similar to that of ^{14}C. This finding suggests that xylem-to-phloem transfer, presumably occurring in the bottom part of the stem, is more active for sulfate transport than for other ions in the mature Arabidopsis plants. The phloem-localizing high affinity sulfate transporter, Sultr1;3, mediates sulfate transport from the cotyledon to other distal organs in Arabidopsis (Yoshimoto et al. 2003). However, to date, the molecular mechanism of sulfate transfer from xylem to phloem is unknown. In addition to sulfate, it is possible to detect other chemical forms of ^{35}S by RRIS. For example, glutathione (GSH) is the most abundant chemical as an organic sulfur compound in phloem sap. Determination of the chemical forms of ^{35}S as well as ^{32}P within the period of live imaging should be a future challenge and one that would allow a deeper understanding of ion transport.

Our study further adds to the variety of ion movement patterns identified among different plant species. In rapeseed, accumulation of ^{32}P at the center of the pod and accumulation of ^{35}S at the tips have been reported (Nakanishi et al. 2009), but these were not significant in Arabidopsis siliques (**Fig. 2a**). In rice plants, ^{32}P and ^{35}S were distributed all over the shoot 15 min after root absorption, and even ^{45}Ca was transported throughout the shoot within 48 h (Kobayashi et al. 2013a), exhibiting a clear contrast to the intense accumulation of ^{45}Ca at the basal part of the Arabidopsis inflorescence (**Fig. 2b**). ^{52}Mn was distributed all over the shoot of barley (Tsukamoto et al. 2006), which contrasts greatly with our data in Arabidopsis (**Fig 2b**). Overall, it appears that monocots transport divalent cations more readily through the upper part of the plant than does Arabidopsis. The different transport patterns observed among the plant species suggest the participation of plant-specific vascular transport systems in the control of long-distance ion transport.

Sink and source tissues determined by tracing foliarly introduced $^{14}CO_2$

Several experiments introducing CO_2 to plants have employed a solid container made of glass or acrylic resin (Mahon et al. 1974, Donahue et al. 1997). While this is useful for supplying the gas easily to the whole plant body, it is less appropriate for targeting to a specific tissue or organ. We therefore used a polyethylene bag to cover specific target tissues (e.g. rosette leaves, inflorescences or whole shoots), and to supply $^{14}CO_2$ because the bag can be easily fitted to suit a variety of tissue shapes. Introduction of the foliar $^{14}CO_2$ application system provided evidence for a change in the direction of phloem flow with the growth stage of the inflorescence. Rosette leaves were shown to be the sole source organs for young stems and roots (**Fig. 4b**). After a period of stem growth, its further growth could be supported by the photosynthates generated by the stem infrastructure itself, independent of the rosette leaves.

In roots of 14-day-old Arabidopsis plants, ^{14}C-labeled photosynthates preferentially accumulated in the tip areas (**Fig. 8c**). This result is in agreement with previous findings in 6-day-old *Brassica napus* seedlings in which the photosynthate produced in leaves was translocated to the meristematic root regions (Dennis et al. 2010). The phloem unloading activity around the root tip of Arabidopsis has been previously visualized

using the carboxyfluorescein (CF) dye applied to a single cotyledon (Oparka et al. 1994). Based on sequential CF images taken by confocal laser scanning microscopy, the protophloem located 200–700 μm behind the root tip was suggested by the authors to function in phloem unloading and subsequent lateral transport. Consistent with this, a high ^{14}C signal intensity was detected around 200 and 800 μm distal to the main root tip using micro-RRIS (**Fig. 8c**). This region, now suggested to be the major sink tissue in roots, can be considered as the part extending from the middle part of the apical meristem to the start of the elongation zone.

To investigate further the dynamics of phloem unloading of photosynthates, micro-RRIS needs to be improved such that plant samples can be supplied with labeled gas and imaged under light conditions. However, the detection of a gaseous radionuclide in macro-RRIS could drastically enhance the versatility of RRIS.

In summary, RRIS allows the movement of the various ions and photosynthates to be temporally analyzed in a whole plant. Thus, RRIS could be a particularly effective apparatus for the study of plant responses to changing environments and stress. Further scope for RRIS application could be in the study of stress responses to a variety of rapidly changing environmental conditions such as temperature, moisture and light.

Materials and Methods

Visualization of eight elements in roots to above-ground parts

Seeds of *Arabidopsis thaliana* Col-0 were grown in full-nutrient culture solution (Fujiwara et al. 1992) at 22°C under 16 h/8 h light/dark conditions with 100 μmol m^{-2} s^{-1} of light. After 43 d, plants approximately 25 cm in height were selected and transferred to 20 ml of culture solution containing radioactive tracer of individual nutritional elements. The tracer concentrations applied were as follows: $^{22}Na^{+}$, 25 kBq ml^{-1}; $^{28}Mg^{2+}$, 15 kBq ml^{-1}; ^{32}P-phsphate, 50 kBq ml^{-1}; ^{35}S-sulfate, 500 kBq ml^{-1}; $^{42}K^{+}$, 1 kBq ml^{-1}; $^{45}Ca^{2+}$, 250 kBq ml^{-1}; $^{54}Mn^{2+}$, 50 kBq ml^{-1}; and $^{137}Cs^{+}$, 25 kBq ml^{-1}. $^{28}Mg^{2+}$ was produced by ^{27}Al (α, 3p) ^{28}Mg reaction and was separated from the Al target (Tanoi et al. 2011). With $^{42}K^{+}$, this element was prepared from an ^{42}Ar–^{42}K generator by milking (Aramaki et al. 2015).

The imaging area was between 3 and 22 cm of the above-ground parts. Samples were irradiated under a light intensity of 100 μmol m^{-2} s^{-1} for 15 min at intervals of 15 min. During each 15 min interval, imaging was performed without light. The radiation converted to photons by the scintillator was harvested for 15 min with a highly sensitive CCD camera (C3077-70, Hamamatsu Photonics Co.). This light and dark irradiation imaging cycle was previously described by Hirose et al. (2013). The signal intensity of each cumulative image was corrected according to its half-life with Image J software. To analyze the velocity of each ion in the direction of the main stem tip, two ROIs were set as follows: ROI:A was 30 mm apart from the uppermost node, ROI:B was 30 mm higher than the ROI:A. Two seedlings were analyzed for each ion experiment. The lower LOQ and the detection limits were defined as 10σ and 3σ, respectively, where σ represents the standard deviation of the background signal intensity.

Heat-girdling treatment

Arabidopsis was grown as described above for imaging of the eight elements. The main stem was heated for several seconds by a soldering iron. The tracer concentrations applied were as follows, $^{14}CO_2$, 1 MBq; ^{32}P-phosphate, 25 kBq ml^{-1}; and $^{28}Mg^{2+}$, 10 kBq ml^{-1}. The plants supplied with $^{14}CO_2$ to rosette leaves were analyzed using IP, while ^{28}Mg and ^{32}P content were determined by RRIS for 24 h.

Visualization of ^{14}C-labeled photosynthate movement from rosette leaves to above-ground parts of Arabidopsis

$^{14}CO_2$ was produced by mixing 2 MBq of ^{14}C-labeled sodium hydrogen carbonate and lactic acid in a 1.5 ml vial with a septum stopper equipped with a syringe needle. Plant samples were transferred to a 100 ml plastic pod containing culture solution. Individual rosette leaves were covered with a polyethylene bag. The mouth of the bag was sealed with clay and a tube was connected to the bag to introduce $^{14}CO_2$ generated in the vial. $^{14}CO_2$ was introduced into the bag for 24 h for successive imaging. The system was irradiated with light during 15 min intervals, and imaging was performed during the alternating 15 min dark intervals. After 24 h of imaging, the sample was placed on an IP for 60 min.

Visualization of $^{14}CO_2$ supplied to different plant tissues and organs

Arabidopsis was grown as described above and, after 30 d, approximately 15 cm above-ground sections of plants were selected for analysis, with tissue areas of between 6 and 15 cm being used for imaging in RRIS. $^{14}CO_2$ was produced by the same method as that for ^{14}C-labeled photosynthates from rosette leaves. Individual rosettes, aerial organs (inflorescences) or whole shoots were covered with a polyethylene bag 1.2 μm in thickness that was sealed with clay, and with a tube connected to the bag to introduce the $^{14}CO_2$ generated into the vial. $^{14}CO_2$ was introduced into the bag for 24 h for successive imaging. The system was irradiated with light during 15 min intervals, and imaging was performed during the alternating 15 min dark intervals.

To fix the sample to a FOS, where the CsI (Tl) scintillator was deposited, a silicone gum sheet was used, and the FOS was covered with polyphenylene sulfide film to prevent contamination with ^{14}C. In the pulse experiment, $^{14}CO_2$ was introduced for 1 h under light irradiation in a phytotron and then ^{14}C movement was imaged for another 48 h.

Foliar supply of $^{14}CO_2$ was performed to visualize leaf-to-root movement of photosynthates, using 14-day-old Arabidopsis seedlings. Plants were grown in a 0.4% gellan gum and full-nutrient culture solution using a dish provided with several vent holes, and the culture conditions were as described for the previous experiment. Plant roots were then placed on a gellan gum on a polyethylene sheet (10 μm thick) for imaging. Then, plants on the FOS were placed vertically, and images were acquired for 15 min at intervals of 1 h. Illumination was supplied by light-emitting diode light (100 μmol m^{-2} s^{-1}) for 45 min between image acquisition periods.

Root elongation measurements

Primary root lengths were measured twice with a 12 h interval on day 14 after germination so that the root elongation rate could be calculated. Five seedlings were used for each measurement.

Micro-RRIS system

The principle of visualization was the same as that for RRIS. An electron-multiplying CCD camera (iXon3 888, Andor Technology Ltd.) was used and microscopic observations were performed with a ×10 objective lens.

Supplementary data

Supplementary data are available at PCP online.

Funding

This work was supported by the Japan Society for the Promotion of Science (JSPS) [through the Funding Program for Next Generation World-Leading Researchers (GS007), JSPS

KAKENHI Grant No. 15H02469 to T.M.N., and 15k18761 to R.S.]; the Japan Science and Technology Agency (JST) [PRESTO to K.T.].

Disclosures

The authors have no conflicts of interest to declare.

References

Antoch, G., Vogt, F.M., Freudenberg, L.S., Nazaradeh, F., Goehde, S.C., Barkhausen, J., et al. (2003) Whole-body dual-modality PET/CT and whole-body MRI for tumor staging in oncology. *JAMA* 290: 3199–3206.

Aramaki, T., Sugita, R., Hirose, A., Kobayashi, N.I., Tanoi, K. and Nakanishi, T.M. (2015) Application of ^{42}K to Arabidopsis tissues using real-time radioisotope imaging system (RRIS). *Radioisotopes* 64: 169–176.

De Schepper, V., Bühler, J., Thorpe, M., Roeb, G., Huber, G., van Dusschoten, D., et al. (2013) ^{11}C-PET imaging reveals transport dynamics and sectorial plasticity of oak phloem after girdling. *Front. Plant Sci.* 4: 200–209.

Dennis, P.G., Miller, A.J. and Hirsch, P.R. (2010) Are root exudates more important than other sources of rhizodeposits in structuring rhizosphere bacterial communities? *FEMS Microbiol. Ecol.* 72: 313–327.

Donahue, R., Poulson, M. and Edwards, G. (1997) A method for measuring whole plant photosynthesis in Arabidopsis thaliana. *Photosynth. Res.* 52: 263–269.

Fujimaki, S., Suzui, N., Ishioka, N.S., Kawachi, N., Ito, S., Chino, M., et al. (2010) Tracing cadmium from culture to spikelet: noninvasive imaging and quantitative characterization of absorption, transport, and accumulation of cadmium in an intact rice plant. *Plant Physiol.* 152: 1796–1806.

Fujiwara, T., Hirai, M.Y., Chino, M., Komeda, Y. and Naito, S. (1992) Effects of sulfur nutrition on expression of the soybean seed storage protein genes in transgenic petunia. *Plant Physiol.* 99: 263–268.

Hirose, A., Yamawaki, M., Kanno, S., Igarashi, S., Sugita, R., Ohmae, Y., et al. (2013) Development of a ^{14}C detectable real-time radioisotope imaging system for plants under intermittent light environment. *J Radioanal. Nucl.* 296: 417–422.

Ishikawa, S., Suzui, N., Ito-Tanabata, S., Ishii, S., Igura, M., Abe, T., et al. (2011) Real-time imaging and analysis of difference in cadmium dynamics in rice cultivars (Oryza sativa) using positron-emitting ^{107}Cd tracer. *BMC Plant Biol.* 11: 172.

Jahnke, S., Menzel, M.I., van Dusschoten, D., Roeb, G.W., Bühler, J.Minwuyelet, S. et al (2009) Combined MRI-PET dissects dynamic changes in plant structures and functions. *Plant Journal* 59: 634–644.

Kanno, S., Yamawaki, M., Ishibashi, H., Kobayashi, N.I., Hirose, A., Tanoi, K., et al. (2012) Development of real-time radioisotope imaging systems for plant nutrient uptake studies. *Philos. Trans. R. Soc. B: Biol. Sci.* 367: 1501–1508.

Kiser, M.R., Reid, C.D., Crowell, A.S., Phillips, R.P. and Howell, C.R. (2008) Exploring the transport of plant metabolites using positron emitting radiotracers. *HFSP J.* 2: 189–204.

Kiyomiya, S., Nakanishi, H., Uchida, H., Nishiyama, S., Tsukada, H., Ishioka, N., et al. (2001) Light activates $H_2{}^{15}O$ flow in rice: detailed monitoring using a positron-emitting tracer imaging system (PETIS). *Physiol. Plant.* 113: 359–367.

Kawachi, N., Suzui, N., Ishii, S., Ito, S., Ishioka, N.S., Yamazaki, H., et al. (2011) Real-time whole-plant imaging of ^{11}C translocation using positron-emitting tracer imaging system. *Nucl. Instrum. Methods Phys. Res. A* 648: S317–S320.

Kobayashi, N.I., Iwata, N., Saito, T., Suzuki, H., Iwata, R., Tanoi, K., et al. (2013a) Different magnesium uptake and transport activity along the rice root axis revealed by ^{28}Mg tracer experiments. *Soil Sci. Plant Nutr.* 59: 149–155.

Kobayashi, N.I., Tanoi, K., Hirose, A. and Nakanishi, T.M. (2013b) Characterization of rapid intervascular transport of cadmium in rice stem by radioisotope imaging. *J. Exp. Bot.* 64: 507–517.

Mahon, J.D., Fock, H. and Canvin, D.T. (1974) Changes in specific radioactivity of sunflower leaf metabolites during photosynthesis in $^{14}CO_2$ and $^{12}CO_2$ at three concentrations of CO_2. *Planta* 120: 245–254.

Marschner, H. (1995) Mineral Nutrition of Higher Plants, 2nd edn. Academic Press, New York.

Matsuhashi, S., Fujimaki, S., Kawachi, N., Sakamoto, K., Ishioka, N. and Kume, T. (2005) Quantitative modeling of photoassimilate flow in an intact plant using the Positron Emitting Tracer Imaging System (PETIS). *Soil Sci. Plant Nutr.* 51: 417–423.

Matsuhashi, S., Fujimaki, S., Uchida, H., Ishioka, N. and Kume, T. (2006) A new visualization technique for the study of the accumulation of photoassimilates in wheat grains using [^{11}C]CO_2. *Appl. Radiat. Isot.* 64: 435–440.

Metzner, R., Thorpe, M.R., Breuer, U., Blüemler, P., Schurr, U., Schneider, H.U., et al. (2010) Contrasting dynamics of water and mineral nutrients in stems shown by stable isotope tracers and cryo-SIMS. *Plant Cell Environ.* 33: 1393–1407.

Minchin, P.E.H. and Thorpe, M.R. (2003) Using the short-lived isotope ^{11}C in mechanistic studies of photosynthate transport. *Funct. Plant Biol* 30: 831–841.

Nakanishi, T., Tanoi, K., Yokota, H., Kang, D., Ishii, R., Ishioka, N., et al. (2001) ^{18}F used as tracer to study water uptake and transport imaging of a cowpea plant. *J. Radioanal. Nucl.* 249: 503–507.

Nakanishi, T.M., Yamawaki M., Ishibashi H. and Tanoi K. (2011) Real-time imaging of ^{35}S sulfate uptake in a rape seed plant. *Proc. Radiochem. A Suppl. Radiochim/ Acta* 1: 293.

Nakanishi, T.M., Yamawaki, M., Kannno, S., Nihei, N., Masuda, S. and Tanoi, K. (2009) Real-time imaging of ion uptake from root to above-ground part of the plant using conventional beta-ray emitters. *J. Radioanal. Nucl. Chem.* 282: 265–269.

Ohtake, N., Sato, T., Fujikake, H., Sueyoshi, K., Ohyama, T., Ishioka, N., et al. (2001) Rapid N transport to pods and seeds in N-deficient soybean plants. *J. Exp. Bot.* 52: 277–283.

Oparka, K.J., Duckett, C.M., Prior, D.A.M. and Fisher, D.B. (1994) Real-time imaging of phloem unloading in the root tip of Arabidopsis. *Plant J.* 6: 759–766.

Phelps, M.E. (2000) Positron emission tomography provides molecular imaging of biological processes. *Proc. Natl. Acad. Sci. USA* 97: 9226–9233.

Schaller, B. (2004) Usefulness of positron emission tomography in diagnosis and treatment follow-up of brain tumors. *Neurobiol. Dis.* 15: 437–448.

Sugita, R., Kobayashi, N.I., Hirose, A., Tanoi, K. and Nakanishi, T.M. (2014) Evaluation of in vivo detection properties of ^{22}Na, ^{65}Zn, ^{86}Rb, ^{109}Cd and ^{137}Cs in plant tissues using real-time radioisotope imaging system. *Phys. Med. Biol.* 59: 837.

Suwa, R., Fujimaki, S., Suzui, N., Kawachi, N., Ishii, S., Sakamoto, K., et al. (2008) Use of positron-emitting tracer imaging system for measuring the effect of salinity on temporal and spatial distribution of ^{11}C tracer and coupling between source and sink organs. *Plant Sci.* 175: 210–216.

Tanoi, K., Saito, T., Iwata, N., Ohmae, Y., Hirose, A., Kobayashi, N.I., et al. (2011) The preparation of ^{28}Mg and analysis of Mg uptake in rice plant. *Radioisotopes* 60: 299–304.

Tsukamoto, T., Nakanishi, H., Kiyomiya, S., Watanabe, S., Matsuhashi, S., Nishizawa, N.K., et al. (2006) ^{52}Mn translocation in barley monitored using a positron-emitting tracer imaging system. *Soil Sci. Plant Nutr.* 52: 717–725.

Tsukamoto, T., Nakanishi, H., Uchida, H., Watanabe, S., Matsuhashi, S., Mori, S., et al. (2009) ^{52}Fe translocation in barley as monitored by a positron-emitting tracer imaging system (PETIS): evidence for the direct translocation of Fe from roots to young leaves via phloem. *Plant Cell Physiol.* 50: 48–57.

Véry, A.A. and Sentenac, H. (2003) Molecular mechanisms and regulation of K^+ transport in higher plants. *Annu. Rev. Plant Biol.* 54: 575–603.

Yamaji, N. and Ma, J.F. (2009) A transporter at the node responsible for intervascular transfer of silicon in rice. *Plant Cell* 21: 2878–2883.

Yoshimoto, N., Inoue, E., Saito, K., Yamaya, T. and Takahashi, H. (2003) Phloem-localizing sulfate transporter, Sultr1;3, mediates re-distribution of sulfur from source to sink organs in Arabidopsis. *Plant Physiol.* 131: 1511–1517.

Weisenberger, A.G., Kross, B., Lee, S., McKisson, J., McKisson, J.E., Xi, W., et al. (2012) PhytoBeta imager: a positron imager for plant biology. *Phys. Med. Biol.* 57: 4195.

Wu, H. and Tai, Y. (2011) A novel phoswich imaging detector for simultaneous beta and coincidence-gamma imaging of plant leaves. *Phys. Med. Biol.* 56: 5583.